Nuclear Physics B129 (1977) 365–389

CHARGED PARTICLE MULTIPLICITY DISTRIBUTIONS IN pp COLLISIONS AT ISR ENERGIES

W. THOMÉ, K. EGGERT, K. GIBONI and H. LISKEN
III. Physikalisches Institut der Technischen Hochschule, Aachen, Germany

P. DARRIULAT, P. DITTMANN †, M. HOLDER and K.T. MCDONALD *
CERN, Geneva, Switzerland

H. ALBRECHT, T. MODIS ** and K. TITTEL
Institut für Hochenergiephysik, Heidelberg, Germany

H. PREISSNER, P. ALLEN ***, I. DERADO, V. ECKARDT, H.-J. GEBAUER, R. MEINKE, P. SEYBOTH and S. UHLIG
Max-Planck-Institut für Physik und Astrophysik, München, Germany

Received 24 June 1977
(Revised 29 July 1977)

We present the first direct measurements of charged-particle multiplicity distributions for pp collisions at ISR energies. The measurements are performed by means of a streamer chamber detector with large solid-angle coverage and excellent multitrack efficiency. Particle densities are observed to rise in the central region as $\sqrt{s}$ increases. The multiplicity distributions in this region deviate from a Poisson law, thus giving evidence for correlations. These correlations are of the same type as those obtained from clustering of the collision products. The mean charged multiplicity over the full rapidity range increases faster than $\log s$. Our data do not support an early onset of KNO multiplicity scaling.

1. Introduction

Earlier ISR experiments have demonstrated the following general properties of proton-proton collisions at very high energy:

the total cross section σ_{tot} increases with the c.m. energy $\sqrt{s}$;

single particle inclusive cross sections obey approximate Feynman scaling with

† Now at DESY, Hamburg, Germany.
* Now at Princeton University, Princeton, New Jersey, USA.
** Now at CEN Saclay, Gif-sur-Yvette, France.
*** Now at Lab. Nazionali di Frascati, Roma, Italy.

limited transverse momenta;

short-range rapidity correlations amenable to a cluster model description are present in the central region;

final states can be qualitatively separated in two classes usually referred to as diffraction and pionization components.

The present work reports on the first direct measurement of the charged-particle multiplicity distribution in the ISR energy range, a quantity which contains implicit information on all above properties of the collision mechanism. Its deviation from a Poisson law reveals correlations, its behaviour at low multiplicities is sensitive to the diffraction component, and its dependence upon $\sqrt{s}$ contains information on the scaling properties of the collision dynamics.

The measurements were performed with two large streamer chambers [1] surrounding an intersection region of the CERN-ISR. Earlier analyses of the data collected with this detector, in particular concerning angular correlations [2] and total cross sections [3], have been previously published. The large solid-angle coverage of the detector and its excellent multitrack efficiency make it an ideal tool to measure charged-particle multiplicities. The absence of a magnetic field precludes particle identification and momentum measurement but a good rejection of charged secondaries not pointing to the production vertex can be achieved.

In the next sections we describe briefly the streamer chamber detector and trigger system (sect. 2), the scanning and measuring procedures (sect. 3) and the corrections applied to the data, as well as the systematic uncertainties (sect. 4). In sect. 5 we present charged particle densities in pseudo-rapidity space. The last sections are devoted to the study of multiplicity distributions and of their energy dependence, sect. 6 in the central region and sect. 7 over the full rapidity range.

2. Streamer chamber detector and trigger system

An intersection region of the ISR is surrounded by two double-gap streamer chambers above and below the beam pipes (fig. 1). Apart from the 8 cm gap between the chambers, they cover the full solid angle. Each chamber is 50 cm high, 270 cm long (along the beams), and 125 cm wide (transverse to the beams). The acceptance is limited by the gap between the chambers. Over most of the angular range it remains equal to 95% but falls steeply in the forward direction to zero below 40 mrad. The tracks are photographed through two 8° stereo views recorded on a single 35 mm film.

The apparatus is triggered by a coincidence between large scintillator hodoscopes on each downstream side of the interaction region. This trigger observes a cross section of 33.9 mb (36.4 mb) at $\sqrt{s}$ = 23.6 GeV (62.8 GeV). Only a small fraction (4% on the average) of events with at least one track in the streamer chamber fiducial volume fails to give a trigger.

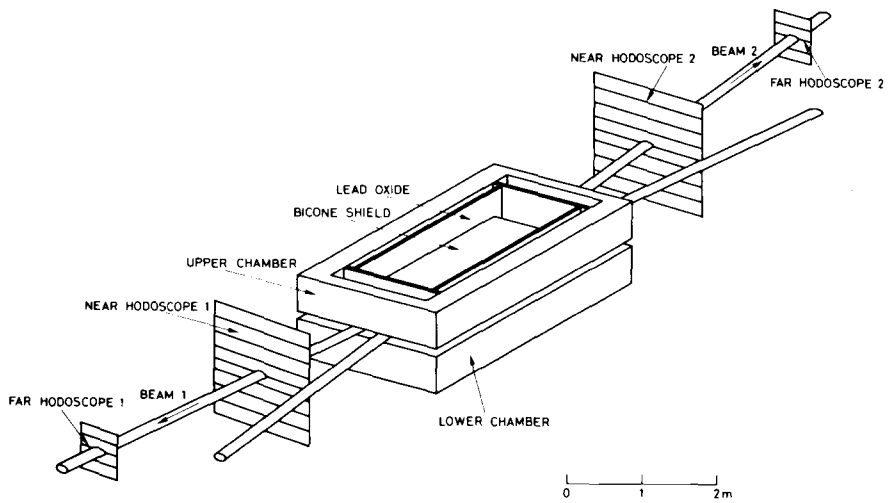

Fig. 1. Schematic layout of the apparatus. Optical system and HV generators have been omitted for clarity.

Detailed descriptions of the trigger efficiency [3] and of the performance of the streamer chambers [1] have been previously published.

3. Data reduction

The film used for this analysis was scanned and measured on image plane digitizers. After rejection of those pictures with a bad high-voltage pulse at the streamer chamber (~15%) and those pictures where a second event had been detected during the sensitive time of the chamber (~3%), the pictures were scanned, excluding those which could not be measured because of too much background (~1%) or because of flares obscuring large parts of the event (~1%). We have checked that this rejection procedure did not bias the sample of retained events.

For all tracks pointing to the interaction region, within a distance corresponding to approximately 17 cm in real space, three points were measured in each view. The tracks were then reconstructed as straight lines in space using both stereo views. The interaction point was found by an iterative least squares fit to all reconstructed tracks: at each iteration the worst tracks were rejected until all remaining tracks fitted to a common vertex within 2 standard deviations. Finally all tracks were refitted using the vertex as an additional point. For the track selection both measurement errors and multiple Coulomb scattering were taken into account. All events were scanned a second time to check the first measurement; partial or complete remeasurements were performed in cases of disagreement. A film containing approximately 500 events has been processed independently in two of the labora-

tories. The numbers of accepted tracks were found to agree to better than 2%. A total of 26 000 events were retained for further analysis, distributed over the five ISR energies as follows: 5903 at $\sqrt{s}$ = 23.6 GeV, 3446 at $\sqrt{s}$ = 30.8 GeV, 2311 at $\sqrt{s}$ = 45.2 GeV, 7385 at $\sqrt{s}$ = 53.2 GeV and 5393 at $\sqrt{s}$ = 62.8 GeV.

The vertex test could not be applied to events with only one observed track: these were however retained in the analysis by assuming a rejection rate equal to that observed in 3- and 4-prong events. The decreased (or missing) vertex constraint for the events with 2 or less tracks was accounted for by increasing the Poisson error on the number of observed 1- and 2-prongs by a factor of 3 and 2 respectively.

Steep tracks are viewed end on by the camera and often cause small flares. From a study of their observed angular distribution we have evaluated specific measurement errors for this class of tracks.

4. Corrections and systematic uncertainties

Several effects cause small differences between the true and observed multiplicities. We have specifically considered and accounted for *:

(i) geometrical acceptance;
(ii) low momentum cut-off;
(iii) nuclear interactions in the surrounding material;
(iv) electrons from converted photons or π^0 Dalitz decays;
(v) K_s and Λ decays;
(vi) elastic events.

4.1. Geometrical acceptance

The gap between the streamer chambers where no particles can be detected amounts to about 10% of the total solid angle. The resulting geometrical acceptance is shown in fig. 2 as a function of the pseudo-rapidity $\eta = -\log \tan\frac{1}{2}\theta$ (θ is the production angle). It remains above 95% in the central region ($|\eta| < 2$) but drops steeply at small angles and vanishes for pseudo-rapidities $|\eta| > 4$. Advantage was taken of the azimuthal symmetry of the final state to calculate the probability matrix p_{nm} for an event with observed multiplicity m to correspond to a true multiplicity n. The calculation was performed by applying random azimuthal rotations to observed events and evaluating each time the decrease of the track multiplicity. The advantage of this method is that we do not rely on any model or multiplicity distribution and that correlations between particles are automatically taken into account. However, the method fails at very forward angles ($|\eta| > 4$); for tracks in this region a special treatment has been applied (see sect. 7). At the lowest energy we have also used FNAL bubble chamber events [5], where the directions of all charged particles are

* For further details see ref. [4].

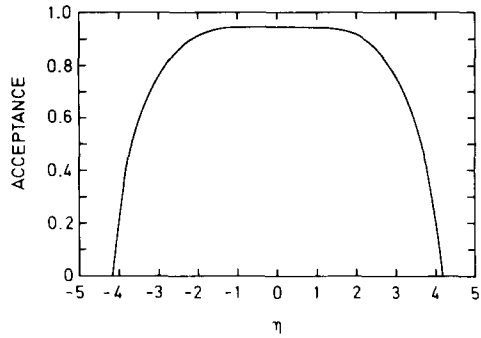

Fig. 2. Geometrical acceptance as a function of c.m. pseudo-rapidity.

known, to obtain an independent evaluation of p_{nm}. Both results are in very good agreement (fig. 3).

4.2. Low momentum cut-off

The particles have to traverse the vacuum chamber walls of the ISR and streamer chamber walls before reaching the sensitive volume. The fraction of particles stopping in this material was calculated from range energy tables [6] by assuming a

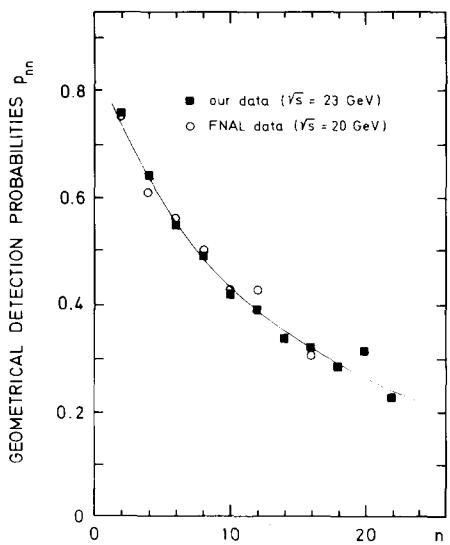

Fig. 3. Probabilities p_{nn} to observe n particles of a produced n-prong event in the streamer chamber detector for our data at $\sqrt{s}$ = 23 GeV (crosses) and FNAL data (open circles). The solid line is a fit to our data.

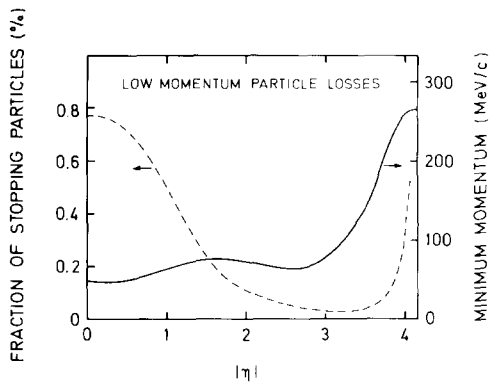

Fig. 4. Low momentum cut-off calculated for pions (solid line) and associated fraction of undetected particles (dashed line) as a function of c.m. rapidity.

transverse momentum distribution $d\sigma/dp_T^2 \propto e^{-6p_T}$ and a Gaussian rapidity distribution. We find that on the average pions are detected down to a momentum of 45 MeV/c (fig. 4). The resulting losses amount to less than 0.5%.

4.3. Nuclear interactions in surrounding material

We have used the method of Gluckstern [7] to evaluate elastic and quasielastic interactions in the vacuum chamber and streamer chamber walls. For low-momentum particles the nuclear scattering is negligible; at 3 GeV/c this effect is as big as multiple Coulomb scattering and it is taken into account when performing the vertex cut (see sect. 3). For the inelastic part most of the interactions can be identified on the scanning table.

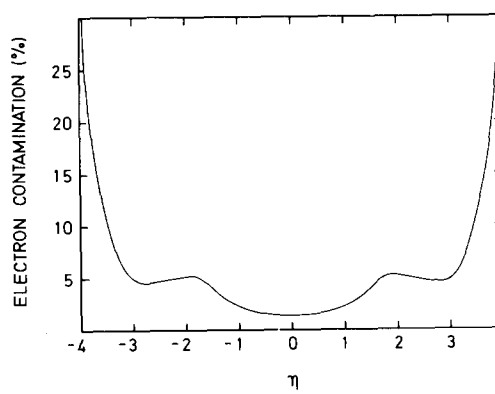

Fig. 5. Percentage of electron contamination calculated as a function of c.m. pseudo rapidity.

4.4. Electron contamination

The observed track sample is partially contaminated by electron and positron tracks coming mostly from the conversion of π^0 decay photons in the vacuum chamber and streamer chamber walls (or internally as Dalitz pairs). We have evaluated the probability for a given observed track to be of that type with the help of photon conversion probability tables [8]. The results, accounting for detailed geometry as well as for measurement and reconstruction uncertainties, are presented in fig. 5.

4.5. K_s and Λ decays

A 2% contamination of additional tracks from $\pi^+\pi^-$ decay of K_s mesons was estimated from existing data [9] and has been taken into account. The contamination due to Λ decays and the losses due to $K^\pm$ decays were found negligible.

4.6. Elastic events

The number of elastic events seen in the streamer chambers has been estimated from published ISR measurements [10] of the elastic cross section. For the higher energies ($\sqrt{s}$ = 45, 53, 63 GeV) this contamination is completely negligible; at the lowest energies ($\sqrt{s}$ = 24, 31 GeV) it amounts to 0.8%, 0.1% and we have reduced the number of 2-prongs accordingly.

4.7. Possible systematic uncertainties

We estimate that the track selection procedure and the corrections described before lead to an uncertainty of 0.25 particles per event. In addition the following effects may cause systematic errors which mainly influence the multiplicity distributions over the full rapidity range:

(i) trigger bias due to the limited acceptance of the scintillator hodoscopes;

(ii) systematic losses at very forward angles.

The magnitude of these effects and the resulting uncertainties on the calculated moments are estimated as follows:

(i) For all energies (except for $\sqrt{s}$ = 23.6 GeV) 7.5% (12%) of the inelastic cross section is missed by our trigger system [3]. The multiplicity distribution for a large part of this cross section has been measured with a special trigger condition, namely by requiring a hit in one of the hodoscopes and none in the other. Multiplicities above 7 are not affected, but smaller multiplicities are enhanced. We have taken this excess to estimate the systematic errors on the moments. The remaining unobserved cross section (2% to 5%) should be of diffractive type and also should only influence the lowest multiplicities. The effect of both types of trigger losses on the multiplicity moments is given in table 1.

(ii) Particles with rapidities $|\eta| > 4$ ($\theta < 40$ mrad) never get into the sensitive

Table 1
Systematic uncertainties on the multiplicity moments due to (i) trigger losses and (ii) forward detection losses

		$\langle n \rangle$	γ_2	γ_3	f_2	f_3	D_2	D_3	C_2	C_3	$\langle n \rangle / D$
A	(i)	−0.44	+0.027	+0.020	+1.3	+7.7	+0.06	+0.09	+0.03	+0.10	−0.08
	(ii)	+0.21	−0.022	−0.008	−2.2	+3.0	−0.14	−0.03	−0.02	−0.07	+0.07
R	(i)	−3.7	+2.7	+2.9	+1.1	+0.7	+0.7	+1.0	+2.7	+3.0	−2.6
	(ii)	+1.8	−2.2	−1.1	−1.8	+0.3	−1.6	−0.3	−2.2	−2.1	+2.3

The uncertainties are given under (A) and their ratios to the statistical errors are listed under (R). The values refer to $\sqrt{s}$ = 63 GeV; the uncertainties decrease with energy and they are negligible at $\sqrt{s}$ = 24 GeV.

volume of the streamer chambers. Therefore the correction for these particles cannot be determined by the rotation method (4.1). The constraint of charge conservation, however, allows the correction of all events with only one particle in this region (see sect. 7.1). We have checked that this was sufficient at $\sqrt{s} = 23.6$ GeV, where we could test the method on bubble chamber events [5]. At higher energies, for low multiplicity events, two or more particles may occasionally escape detection in the forward region. We have estimated these losses from a sample of fake events obtained from the bubble chamber events [5] by scaling particle rapidities proportionally to $\log s$. The results, expressed in terms of uncertainties on the multiplicity moments, are listed in table 1.

5. Rapidity distributions of charged particles

The pseudo-rapidity distributions of charged particles for five different values of $\sqrt{s}$ are presented in fig. 6. The Lorentz transformation from the ISR frame to the c.m. frame was performed under the assumption that all particles are massless. Two main features are observed as $\sqrt{s}$ increases: an extension of the rapidity plateau and an increase of the particle density in the central region.

In order to test the concept of limiting fragmentation [11] and the Feynman scaling hypothesis [12], we transform the measured pseudo-rapidity distribution into the true-rapidity distribution in the following way *: We parametrise the true-rapidity distribution by the 3-parameter formula:

$$\frac{1}{\sigma}\frac{\mathrm{d}\sigma}{\mathrm{d}y} = C\left(1 + \exp\frac{y - y_0}{\Delta}\right)^{-1} . \tag{5.1}$$

Under the assumption that all collision products are pions, and that the transverse momentum distribution factorizes in the form $\mathrm{d}\sigma/\mathrm{d}p_\mathrm{T}^2 \propto \exp\{-6\, p_\mathrm{T}\}$, we determine the three parameters in (5.1) by fitting the measured pseudo-rapidity distribution. The formula (5.1) was chosen to describe conveniently the central plateau and the fall-off in the fragmentation region of the distribution by means of the parameters y_0 and Δ respectively. For all five energies we have found the same fall-off parameter $\Delta = 0.59$, which is in agreement with the earlier observation [14] that the data in the fragmentation region coincide when displayed as a function of y_lab, i.e. the rapidity in the rest system of one of the beam particles.

To investigate this point in more detail we have calculated, for a fixed height of the rapidity distribution, $(1/\sigma)\mathrm{d}\sigma/\mathrm{d}y = \text{const.}$, the corresponding value y' in the rest system of one beam particle. We have chosen the height $(1/\sigma)\mathrm{d}\sigma/\mathrm{d}y = 0.8$ where our acceptance corrections are still small for all energies. The data displayed in fig. 7 as a function of $\log\sqrt{s}$ show a slight increase of y' with energy, indicating a small varia-

* For further details see ref. [13].

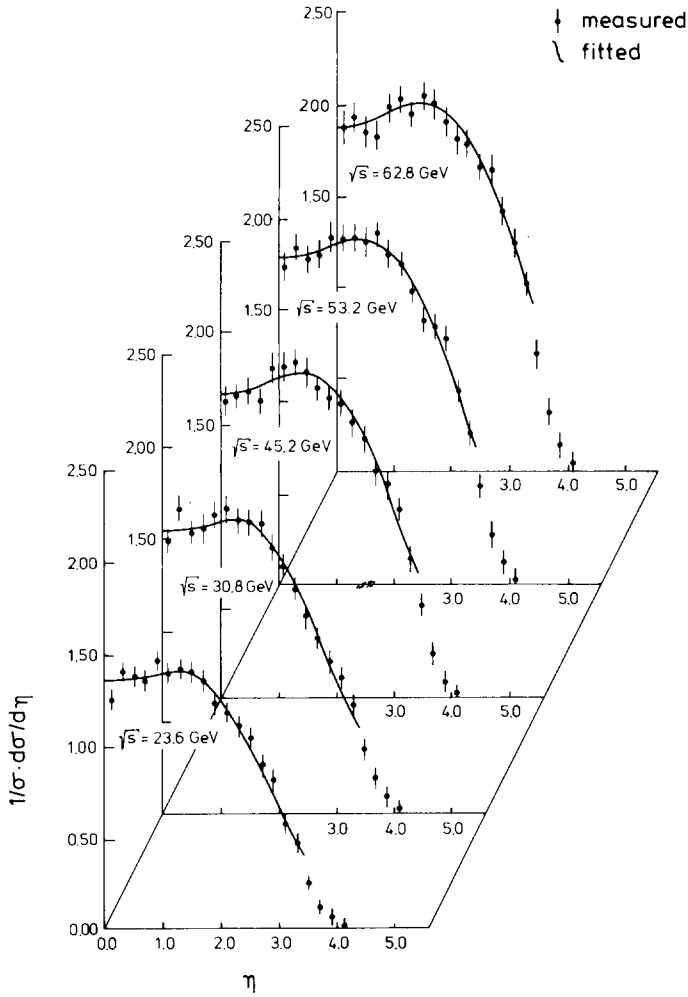

Fig. 6. Pseudo-rapidity distributions in the c.m. system for the different energies. The solid lines are the results of the fits described in the text.

tion of the cross section in the fragmentation region. This result is only significant to the extent that the proton to pion ratio in this region is independent of $\sqrt{s}$.

The density increase in the central region in the ISR energy range has previously been obtained from measurements of single-particle inclusive cross sections using the knowledge of the total pp cross section. Using our fitted rapidity distributions, we have evaluated the quantity $(1/\sigma)\mathrm{d}\sigma/\mathrm{d}y|_{y=0}$ to compare our data with the single particle inclusive measurements of Guettler et al. [15]. In performing this comparison we have accounted for trigger losses (collisions populating the central region but

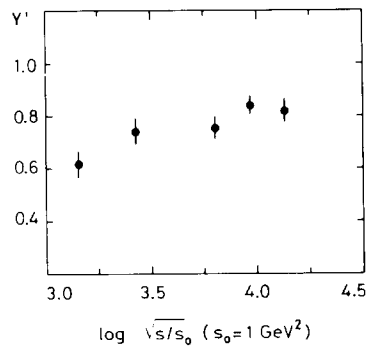

Fig. 7. Rapidity y', measured in the rest system of a beam particle, where the true rapidity distribution crosses the value of 0.8, as a function of $\log \sqrt{s}$.

failing to trigger our detector) and taken as reference energy $\sqrt{s} = 53.2$ GeV where our uncertainties are smallest. In both experiments the low-momentum pion cut-off is approximately 45 MeV/c but the single-particle data are for pions only while all types of stable charged hadrons are included in our sample. The results, presented in fig. 8, display a good agreement between both sets of data, giving further evidence for a substantial violation of Feynman scaling in the central region within the ISR energy range.

In order to get a measure of the rise of the central particle density when averaging over the whole plateau region, we have calculated the mean charged particle multiplicity in the pseudo-rapidity interval $|\eta| < 1.5$. Only events with at least one

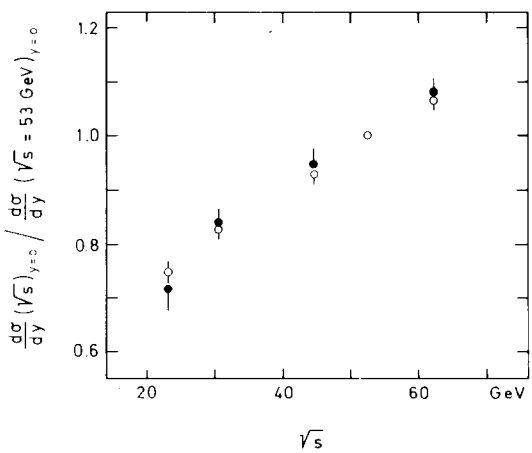

Fig. 8. The ratio $R = d\sigma/dy\ (y = 0, \sqrt{s})/d\sigma/dy\ (y = 0, \sqrt{s} = 53.2)$ as a function of $\sqrt{s}$ from the present analysis (full dots) and from the work of ref. [15] (open circles).

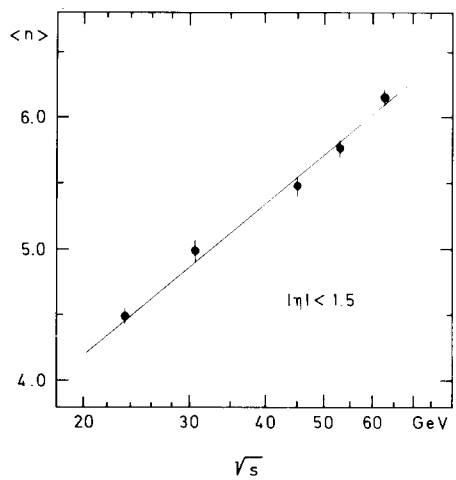

Fig. 9. Mean charged particle multiplicity in the interval $|\eta| < 1.5$ as a function of log s. Only events with at least one track in this interval are considered. The full line is the result of a linear fit of the data.

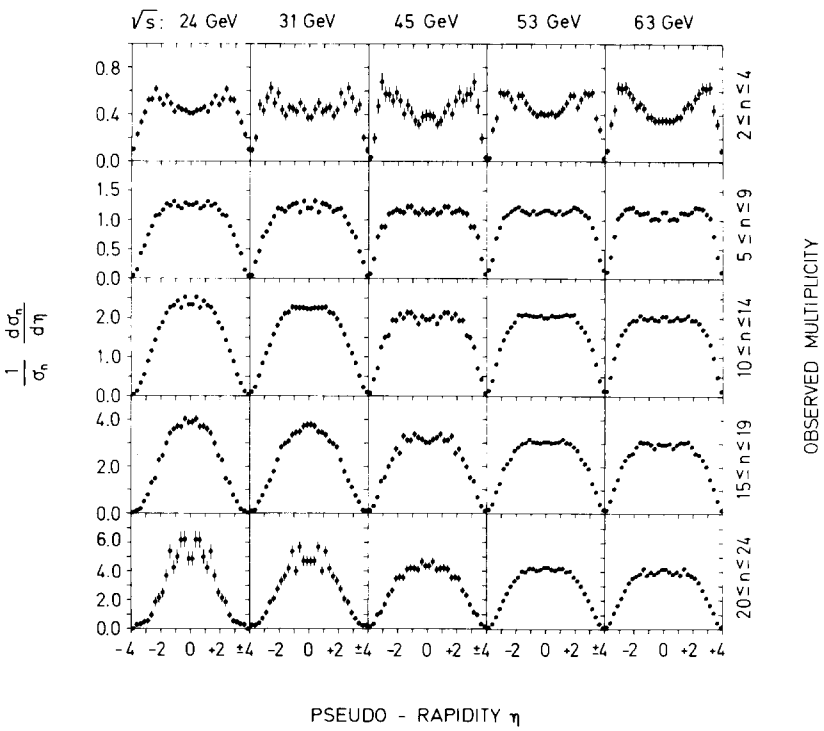

Fig. 10. Normalized charged particle densities (corrected for acceptance up to $|\eta| \simeq 4$) in various intervals of the total observed multiplicity.

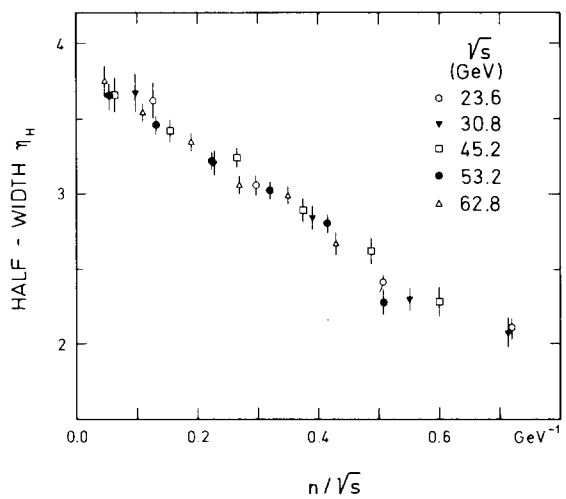

Fig. 11. Half-width at half-maximum of the normalized charged particle densities (fig. 10) as a function of $n/\sqrt{s}$, where n is the observed charged multiplicity in the range $|\eta| < 4$.

charged particle in this interval are considered. A linear rise in log s is observed (see fig. 9) with a slope $dn/d \log s = 0.83 \pm 0.04$.

We have also studied charged particle densities in pseudo-rapidity space as a function of n, where n is the observed multiplicity in the range $|\eta| < 4$. The distributions are displayed in fig. 10. The low multiplicity η-distributions exhibit a double bump structure which becomes more pronounced at higher energies. It is suggestive to assign this structure partly to the fragmentation of the incoming protons. With increasing multiplicities the width of the η-distributions decreases. This shrinkage of the η-distributions obeys an interesting scaling law as seen in fig. 11, where the half-width at half-maximum is observed to depend on the single variable $n/\sqrt{s}$, as can be approximately expected from energy-momentum conservation.

6. Multiplicity distributions in the central region

We have analysed multiplicity distributions in the pseudo-rapidity range $|\eta| < 1.5$, which is wide enough to allow for good statistics and sufficiently remote from the edges of the rapidity plateau to permit a specific analysis of the central region. As before the analysis is restricted to events with at least one particle in the chosen η-range. Our data (fig. 12), displayed as a function of the variable $z = n/\langle n \rangle$, obey approximately semi-inclusive KNO scaling [16], i.e. the normalized multiplicity distribution multiplied by the average multiplicity in this η-region is an energy-independent function of z.

A more sensitive test of the KNO scaling concept and of the inherent informa-

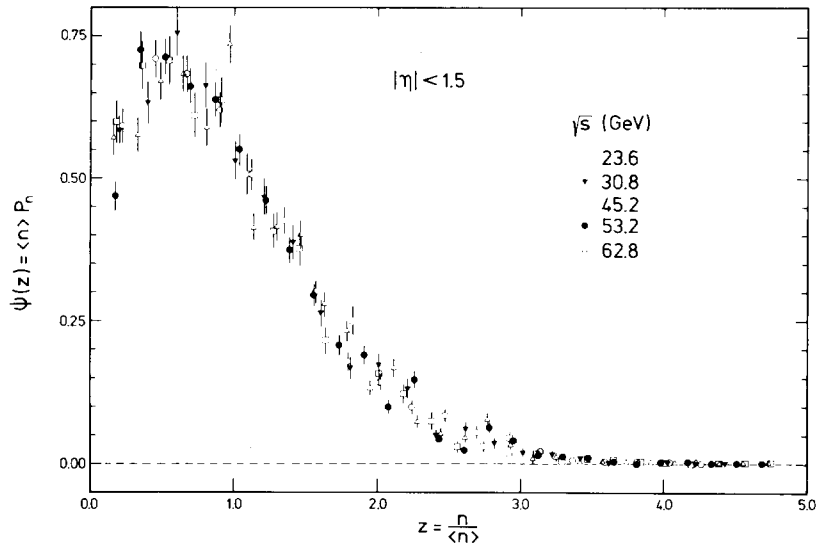

Fig. 12. Normalized multiplicity distributions of charged particles in the central region ($|\eta| < 1.5$) as a function of the KNO variable $z = n/\langle n \rangle$.

tion on correlations was performed in terms of moments, which are integrals of correlation functions. In fig. 13 we show the γ-moments which, in the case of exact KNO scaling, are energy-independent. They are defined as

$$\gamma_2 = \frac{\langle (n - \langle n \rangle)^2 \rangle}{\langle n \rangle^2} = \frac{D_2^2}{\langle n \rangle^2} ,$$

$$\gamma_3 = \frac{\langle (n - \langle n \rangle)^3 \rangle}{\langle n \rangle^3} = \frac{D_3^3}{\langle n \rangle^3} ,$$

$$\gamma_4 = \frac{\langle (n - \langle n \rangle)^4 \rangle - 3\langle (n - \langle n \rangle)^2 \rangle^2}{\langle n \rangle^4} = \frac{D_4^4 - 3D_2^4}{\langle n \rangle^4} . \tag{6.1}$$

The observed values are much higher than the Poisson moments for the same mean multiplicity and are also higher than the corresponding moments for the full rapidity range (sect. 7). This reflects the presence of strong correlations in the central region. The observed moments correspond to the Poisson values for a multiplicity approximately 2.5 times smaller than the actual one, which suggests a description in terms of cluster emission [17]. Therefore we have compared our data with the predictions of the following cluster model [18], which also correctly describes all rapidity correlations [2].

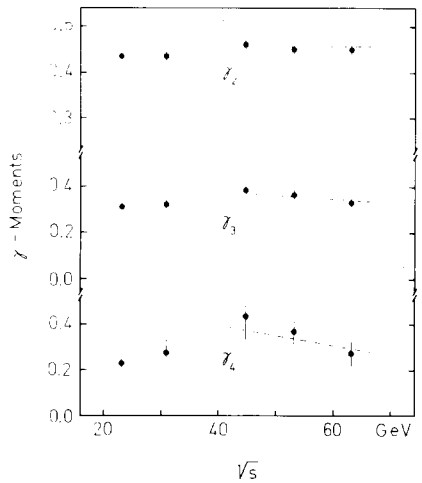

Fig. 13. γ-moments of the multiplicity distribution in the central region ($|\eta| < 1.5$) as a function of $\sqrt{s}$. The dashed lines are obtained from a cluster model with an energy-independent decay multiplicity distribution (see text).

The production of low-mass clusters is described by the matrix element

$$M \propto \frac{E_1 E_2 - p_{L1} p_{L2}}{s} \prod_{k=1}^{n+2} e^{-\lambda \sqrt{m_k^2 + p_{Tk}^2}}, \tag{6.2}$$

where the first term generates the leading particle effect for the nucleons and the product describes the transverse momentum spectra for the n clusters and 2 nucleons. For each event 4-momentum and charge conservation is taken into account. Short-range correlations are obtained by isotropic decay of the clusters in their individual rest systems with a Poisson-like decay multiplicity of mean $\langle k \rangle = 3$, resulting in an average of 2 charged particles per cluster decay. The mass of each cluster depends on its decay multiplicity k and is given by the function $M(\text{GeV}) = \exp(\frac{1}{3}k - 1)$. The resulting average mass $\langle M \rangle = 1.2$ GeV is independent of $\sqrt{s}$. The charged-particle multiplicity distribution is forced to agree with the measured distribution. This requirement introduces correlations between clusters in addition to those arising from 4-momentum conservation. These non-kinematic correlations are rising in strength with energy.

The Monte Carlo calculation reproduces well the change of the γ-moments in comparison with the Poisson values. This result is qualitatively independent of the details of the model. The calculated moments (dashed lines in fig. 13) are in good agreement with experiment at the three higher energies. The Monte Carlo calculation reveals the importance of long-range correlations between clusters (in addition to the well known short-range correlations between particles) if the mean cluster mass is independent of energy.

7. Multiplicity distributions over the full rapidity range

7.1. Determination of the multiplicity distribution

In order to obtain the total charged multiplicity the corrections described in sect. 4 have to be applied. For low multiplicities systematic losses in the very forward direction are important and have to be correctly taken into account. For the higher multiplicities, because of the narrower rapidity distribution (see fig. 10), these losses are small. The method of calculating the true multiplicity distribution is described below:

If v_m is the number of events with m observed tracks and x_n is the unknown number of n-prongs produced, then

$$\sum_n p_{nm} x_n = v_m \,, \tag{7.1}$$

where p_{nm} is the probability to observe a true n-prong as an event with m tracks. We use for the matrix coefficients p_{nm} the experimentally determined detection probabilities (sect. 4), smoothed by some empirically chosen functions (solid lines in fig. 14). This raw matrix is modified to include further corrections, as described in sect. 4, for electron tracks, for decay particles of K^0 mesons and for low-momentum

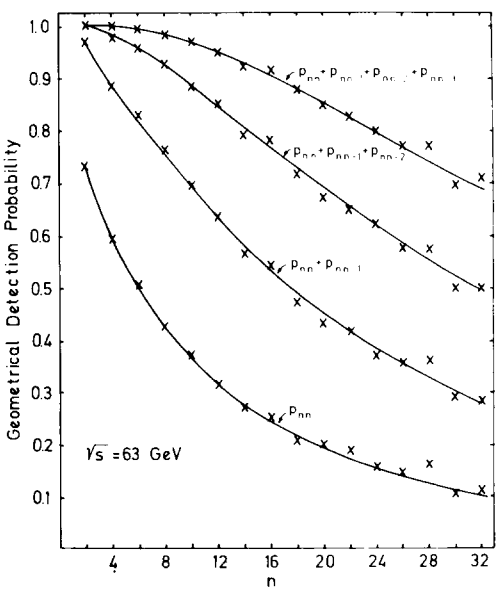

Fig. 14. Accumulated probabilities to observe n, n-1, n-2 and n-3 particles in the streamer chamber detector from a produced n-prong event at $\sqrt{s}$ = 63 GeV. The solid lines are fits to the calculated values.

particles which are stopped before entering the sensitive volume of the detector.

For the numerical solution of the system of equations (7.1) one has to introduce upper limits for both indices n and m. The choice of the cut-offs (as indicated in fig. 15) is a compromise between a large number of degrees of freedom in eq. (7.1) to achieve a good stability for the solution and the maximum information to be extracted from the measurements. The stability of the solution is greatly improved by the constraint of charge conservation on the true multiplicity. To account approximately for the information lost by introducing the cut-off we accumulate all values beyond the cut-off into the last bin. This means for the solution vector that its last component will also contain all events with a multiplicity greater than the cut-off multiplicity. These events are redistributed beyond the cut-off according to $x_n \propto z \exp(-\frac{1}{4}\pi z^2)$ (where $z = n/\langle n\rangle$), the same distribution that provides for the accumulated probabilities p_{nm} at the cut-off.

The enforced charge conservation causes a disagreement with our measurements at low multiplicities. This can be explained by events with one very forward particle, in a region where our acceptance is zero. Such events can be accommodated in the solution of eq. (7.1) if we allow n to take on values 1, 3 and 5 as well as any even number; finally charge conservation is restored by assigning the odd-prong solutions to the next higher even-prong events. Events with two particles missed in the forward region will not be corrected for by this method. (For an estimate of this effect see table 1.)

We minimize

$$\chi^2 = \sum_m \frac{(v_m - \sum_n p_{nm} x_n)^2}{(\Delta v_m)^2} \,, \tag{7.2}$$

Δv_m being the Poisson error of v_m (increased by a factor of 3(2) for $m = 1(2)$), by inversion of the matrix of its derivatives. The inverse matrix is the error matrix which is used for all subsequent error calculations.

7.2. Analysis of the multiplicity distribution

The total charged particle multiplicity distribution implicitly contains information on important properties of the collision mechanism; e.g. its deviations from a Poisson law reveal correlations [19], its dependence upon energy contains information on scaling properties of the reaction mechanisms. One of the striking results at Serpukhov and FNAL energies was the precocious onset of semi-inclusive KNO scaling. Our multiplicity distributions at the five ISR energies are shown in fig. 15. The dashed histograms represent the observed data and the solid-line histograms are the corrected distributions P_n. The curves represent the KNO function

$$\psi(z) = \lim_{s\to\infty} \langle n\rangle \sigma_n(s)/\sigma_{\text{inel}}(s)$$

$$= (3.79z + 33.7z^3 - 6.64z^5 + 0.332z^7)\exp(-3.04z) \tag{7.3}$$

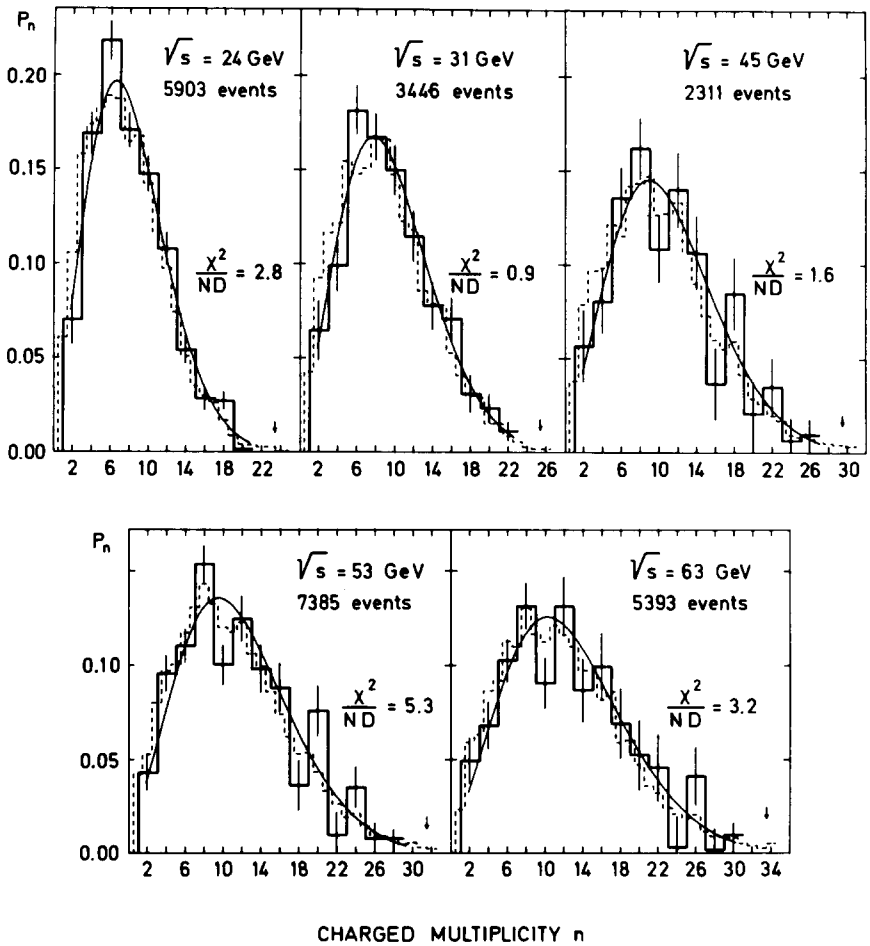

Fig. 15. Total charged particle multiplicity distributions (normalized) for the five ISR energies. The dashed histograms indicate the distributions for raw data (normalized to 2). The solid lines show Slattery's fit to data up to FNAL energies. The chi-squared values of our data to this fit are indicated in the plots.

obtained by Slattery [20] from Serpukhov and FNAL data. The formula is a phenomenological fit to those data to illustrate the consistency with a single energy-independent form. The function also seems to agree with our data, but the chi-squared values (see fig. 15) calculated with the full error matrix indicate some deviation at the higher energies. Only part of the observed deviation is due to the dip seen in the 10-prong channel at the three upper energies. This dip is caused by a depletion in the raw data around $n = 10$. We do not see any experimental bias specific to that region nor does the correction method produce this dip when applied to

Monte Carlo events. The dip has no influence on the multiplicity moments calculated below. We have checked this by artificially smoothing the region around $n = 10$.

There are a few theoretical attempts to derive the ψ-function. In the framework of a unitary uncorrelated cluster model, de Groot [21] obtained the following parameter-free formula:

$$\psi(z) = \frac{3.333z}{(\Gamma(z+1))^2} \exp(-0.892z) . \tag{7.4}$$

While at lower energies the formula gives only a poor description of our data ($\chi^2/\mathrm{ND} = 10.6$ at $\sqrt{s} = 24$ GeV), it describes the data well at higher energies ($\chi^2/\mathrm{ND} \simeq 1.3$ for $\sqrt{s} > 45$ GeV) and shows better agreement with our data than does Slattery's formula (7.3). The good agreement between the data and the model of de Groot indicates the importance of long-range correlations, which are introduced into this model by requiring that the inelastic scattering amplitude is a smooth continuation of the elastic one.

A more detailed analysis of the multiplicity distribution can be performed in terms of moments. The simplest of these moments is the average multiplicity $\langle n \rangle = \Sigma n p_n$ (see fig. 16). Combining lower energy data [22] with ours, we have fitted several energy dependent expressions to $\langle n \rangle$. The formulae used and the results obtained, are shown in table 2 and fig. 16. The agreement of our data with previously published fits [22] is excellent. Furthermore, our data confirm that a simple $a+b \log s$ function is not sufficient to describe the energy dependence of $\langle n \rangle$, which reflects the observed rise of the rapidity plateau (see sect. 5). As described in section 6 we have tested the concept of scaling in terms of the γ-moments (formula (6.1)). For c.m. energies between 10 GeV and 24 GeV these moments are consistent with being constant (fig. 17). The constant value of γ_3 was evidence, according to

Table 2
Fits of energy-dependent expressions to the experimental values of $\langle n \rangle$ including data at lower energies [22]

$\langle n \rangle = f$ (energy)	a	b	c	χ^2/ND
$a\, s^{1/4}$	1.668 ± 0.012			6.8 [a]
$a\, q^b$ [b]	2.181 ± 0.009	0.430 ± 0.003		2.5
$a + b \log s + c (\log s)^2$	0.88 ± 0.10	0.44 ± 0.05	0.118 ± 0.006	1.8
$a + b \log q + c (\log q)^2$ [b]	2.43 ± 0.03	0.36 ± 0.05	0.510 ± 0.014	2.1
$a + b \log s + cs^{-1/2}$	−4.75 ± 0.27	2.03 ± 0.05	8.33 ± 0.60	3.81

[a] Only data for $p_{\mathrm{lab}} > 20$ GeV/c were used for this fit.
[b] q is the kinetic energy $\sqrt{s} - 2m_{\mathrm{p}}$.

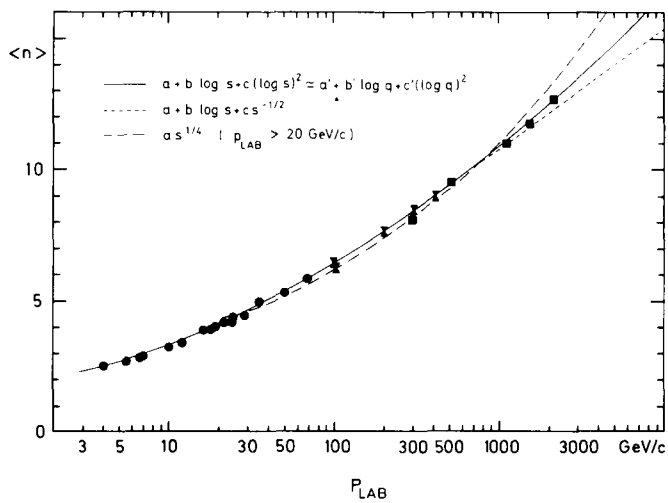

Fig. 16. Mean-value of the total charged multiplicity as a function of p_{lab}. Data from other experiments [22] at lower energies are included.

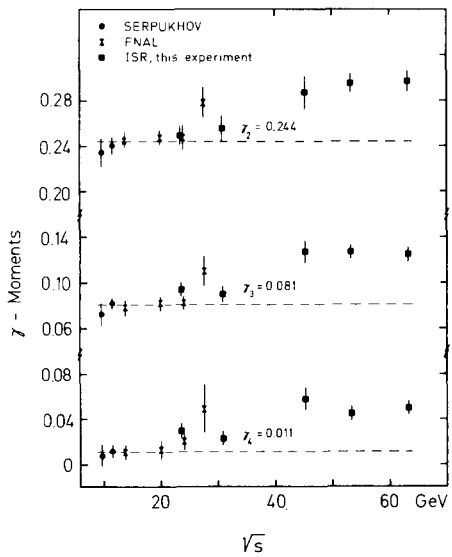

Fig. 17. γ-moments of the total charged multiplicity distributions as a function of $\sqrt{s}$. Data from other experiments at lower energies are included.

Table 3
Various moments and their statistical errors for the total charged multiplicity distributions at the different energies

$\sqrt{s}$ (GeV)	23.6	30.8	45.2	53.2	62.8
$\langle n \rangle$	8.12	9.54	11.01	11.77	12.70
±	0.08	0.12	0.17	0.10	0.12
γ_2	0.249	0.256	0.287	0.295	0.297
±	0.009	0.012	0.015	0.008	0.010
γ_3	0.094	0.090	0.127	0.127	0.125
±	0.006	0.007	0.010	0.006	0.007
γ_4	0.031	0.022	0.058	0.045	0.051
±	0.006	0.006	0.010	0.006	0.006
C_2	1.249	1.256	1.287	1.295	1.297
±	0.009	0.012	0.015	0.008	0.010
C_3	1.840	1.859	1.988	2.012	2.017
±	0.033	0.041	0.054	0.030	0.034
C_4	3.08	3.12	3.53	3.58	3.60
±	0.09	0.11	0.16	0.09	0.10

The moments C_q are defined by $C_q = \langle n^q \rangle / \langle n \rangle^q$.

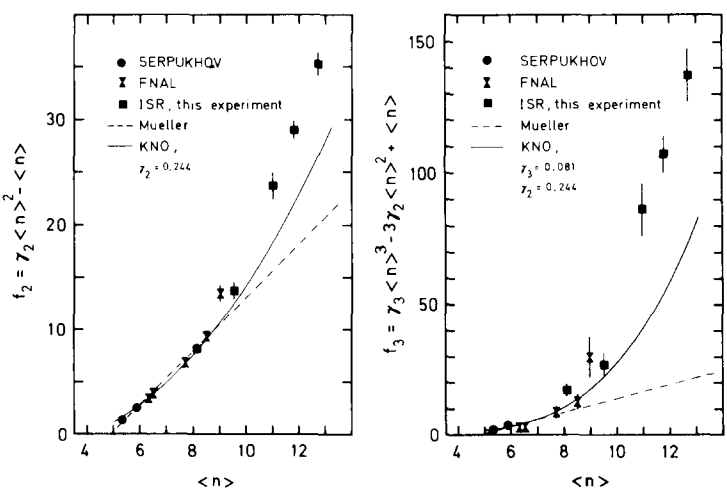

Fig. 18. f-moments of the total charged multiplicity distributions as a function of $\langle n \rangle$. Data from other experiments at lower energies are included. The dashed lines show the predictions of Mueller's Regge-pole dominance model; the solid lines show the predictions from the KNO multiplicity scaling.

Koba and Weingarten [19], for early KNO scaling and against the two component model. Our data show an increase of the γ-moments with energy (fig. 17 and table 3).

In fig. 18 we have plotted the so-called Mueller moments

$$f_2 = \langle n^2 \rangle - \langle n \rangle^2 - \langle n \rangle , \tag{7.5}$$

$$f_3 = \langle n^3 \rangle - 3\langle n \rangle \langle n^2 \rangle - 3\langle n^2 \rangle + 2\langle n \rangle^3 + 3\langle n \rangle^2 + 2\langle n \rangle ,$$

which are some measure of the departure of the multiplicity distribution from the Poisson distribution (for which $f_2 = f_3 = 0$). The dashed lines are the predictions of Mueller's Regge-pole dominance calculations [23] and the solid lines are predictions from semi-inclusive KNO scaling if the constant values of the γ-moments at FNAL energies are assumed. Our data are completely inconsistent with Mueller's prediction and, as already seen in the γ-moments, they do not agree with the early onset of the semi-inclusive KNO scaling either.

For further illustration of our data we show in fig. 19 the dependence of $\langle n \rangle / D$ ($D = D_2$ = dispersion) on the corresponding laboratory momenta, including lower energy data. It can be seen that the ratio $\langle n \rangle / D$ is still decreasing over the ISR energy range.

In fig. 20 we show the moments

$$D_q = \langle (n - \langle n \rangle)^q \rangle^{1/q} , \qquad q = 2, 3, \ldots \tag{7.6}$$

(see eq. (6.1) for comparison) as a function of $\langle n \rangle$. Wroblewski's linear fit [24] of D_2 to data at lower energies extrapolates well through our energies and also for the

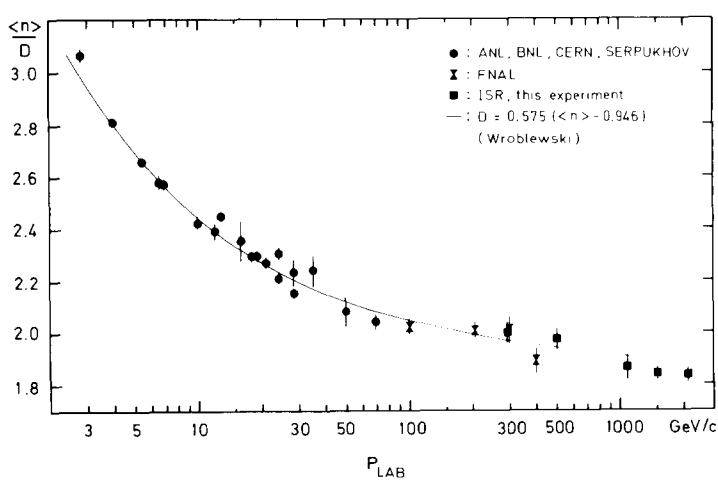

Fig. 19. The ratio $\langle n \rangle / D$ as a function of laboratory momenta. Data from other experiments at lower energies are included.

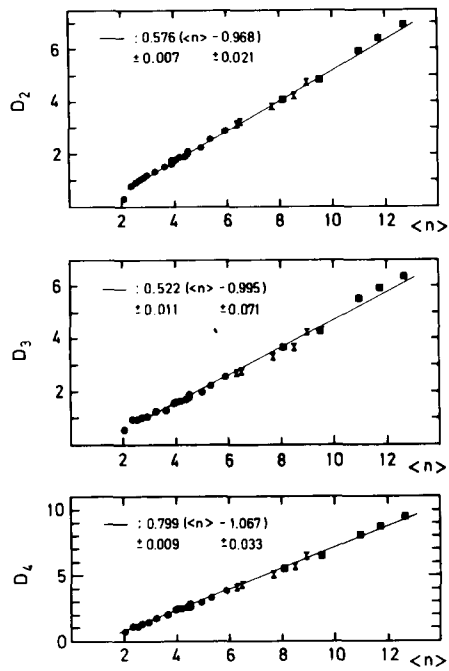

Fig. 20. D_q moments as a function of $\langle n \rangle$. The straight lines are linear fits to the data.

higher moments a linear dependence on $\langle n \rangle$ is observed (fig. 20). In the case of KNO scaling the quantities $D_q/\langle n \rangle$ are constant, but the observed linearity in fig. 20 implies

$$\frac{D_q}{\langle n \rangle} = a_q \left(1 - \frac{\alpha_q}{\langle n \rangle}\right). \tag{7.7}$$

Thus the terms $\alpha_q/\langle n \rangle$ measure the deviation from KNO scaling at finite energies. Alternatively, one can define $z' = (n - \alpha)/\langle n - \alpha \rangle$ rather than $z = n/\langle n \rangle$ as the proper scaling variable at present energies because the observed values of α_q are almost the same for the different values of q ($\alpha_q = 0.97 \ldots 1.07$). This can be interpreted [25] as $n - \alpha$ being the number of actually produced charged particles and α itself being a measure of the average number of charged leading particles.

8. Conclusions

We have presented the first direct measurements of charged particle multiplicity distributions in proton-proton collisions within the ISR energy range.

Our main observations have been:

an increase of particle density in the central region, of the order of 0.28 particles per unit of rapidity and unit of log s, giving evidence for an important violation of Feynman scaling.

a small energy dependence of the particle densities in the fragmentation region, indicating a possible deviation from the prediction of limiting fragmentation.

a decrease of the width of the rapidity distribution with increasing multiplicity n which can be described by a function of the single variable $n/\sqrt{s}$.

an analysis of the multiplicity distribution in the central region by means of moments reveals substantial correlations which are well described in terms of a cluster model; in this model correlations between clusters are important.

For the charged particle multiplicities over the full rapidity range we observe the following features:

the KNO multiplicity scaling suggested by FNAL data does not continue in the ISR energy range and should not be interpreted as an early onset.

the energy dependence of the mean multiplicity $\langle n \rangle$ is best described by a form $\langle n \rangle = a + b \log s + c (\log s)^2$; energy dependences of the form $\langle n \rangle = a + b \log s$ or $\langle n \rangle = a s^{1/4}$ are excluded by our data.

the increase of the moments f_2 and f_3 with $\langle n \rangle$ is much faster than linear and is incompatible with Mueller's Regge-pole dominance calculations.

the linear form $D_q = a_q(\langle n \rangle - \alpha_q)$ observed at lower energies extrapolates well through our energy range; the deviation from the asymptotic values for KNO scaling as measured by the terms $\alpha_q/\langle n \rangle$ is approximately 10%.

We thank Prof. H. Faissner for encouragement and Prof. N. Schmitz for support and useful suggestions. We have benefitted from instructive discussions with M. Le Bellac, J. Benecke, M. Cornelssen, E.H. de Groot, S. Pokorski and A. Wroblewski.

We are indebted to B. Betev, G. Bohm, J. Kaltwasser, H. Pugh, O. Sander and G. Vesztergombi who have made major contributions to the running of the experiment or to its analysis. We also thank the ISR staff for providing excellent operating conditions.

The lengthy task of scanning and measuring has been performed with perseverance and care by the scanning teams in our laboratories. Miss K. Krause, Mrs. G. Lottspeich and Miss I. Wenn have been very helpful in setting up computer programs and supervising the measuring in our laboratories.

Partial financial support was given by the Bundesministerium für Forschung und Technologie.

References

[1] K. Eggert et al., Nucl. Instr. 126 (1975) 477.
[2] K. Eggert et al., Nucl. Phys. B86 (1975) 201.
[3] K. Eggert et al., Nucl. Phys. B98 (1975) 93.
[4] R. Meinke, Thesis, Max-Planck-Institut für Physik und Astrophysik, Munich, Germany.

[5] S. Barish et al., Phys. Rev. D9 (1974) 2689.
[6] W.P. Trower, High-energy particle data, vol. II, Berkeley, Cal., UCRL-2426, 1966.
[7] R.L. Gluckstern, Nucl. Instr. 24 (1963) 381; 56 (1967) 145.
[8] H. Messel and D.F. Crawford, Electron-photon shower distribution function tables for lead, copper and air absorbers, (Pergamon Press, 1970).
[9] B. Alper et al., Phys. Lett. 47B (1973) 275.
[10] U. Amaldi et al., Phys. Lett. 44B (1973) 112;
A. Böhm et al., Phys. Lett. 49B (1974) 491.
[11] J. Benecke, T.T. Chou, C.N. Yang and E. Yen, Phys. Rev. 188 (1969) 2159.
[12] R.P. Feynman, Phys. Rev. Lett. 23 (1969) 1414.
[13] W. Thomé, Thesis, III Physikalisches Institut der TH Aachen, Germany, in preparation.
[14] P. Capiluppi et al., Nucl. Phys. B79 (1974) 189 and references therein.
[15] K. Guettler et al., Phys. Lett. 64B (1976) 111.
[16] Z. Koba, H.B. Nielsen and P. Olesen, Nucl. Phys. B40 (1972) 317.
[17] A. Arneodo and G. Plaut, Nucl. Phys. B107 (1976) 262; B113 (1976) 156.
[18] S. Uhlig, Thesis, Max-Planck-Institut für Physik und Astrophysik, Munich, Germany; in preparation.
[19] Z. Koba, D. Weingarten, Nuovo Cim. Lett. 8 (1973) 303.
[20] P. Slattery, Phys. Rev. Lett. 29 (1972) 1624.
[21] E.H. de Groot, Phys. Lett. 57B (1975) 159.
[22] J. Whitmore, Phys. Reports 5 (1974) 273; 27 (1976) 188;
E. Albini et al., Nuovo Cim. A32 (1976) 101.
[23] A.H. Mueller, Phys. Rev. D4 (1971) 150.
[24] A. Wroblewski, Phys. Reports, to be published.
[25] R. Møller, Nucl. Phys. B74 (1974) 145 and references therein.